UNIVERSITY OF
BATH

Link to publication

University of Bath

Solid-gas phase photo-catalytic behaviour of rutile and TiOn (1<n<2) sub-oxide phases for self-cleaning applications

Manuel Nuño [1], Vaia Adamaki [2], David M. Tobaldi [3], Maria J. Hortigüela Gallo [4], Gonzalo Otero-Irurueta [4], Chris R. Bowen [2] and Richard J. Ball [1,*]

[1] BRE Centre for Innovative Construction Materials (CICM), Department of Architecture and Civil Engineering, University of Bath, Claverton Down, BA2 7AY, UK

[2] Department of Mechanical Engineering, University of Bath, Claverton Down, BA2 7AY, UK

[3] Department of Materials and Ceramic Engineering/CICECO—Aveiro Institute of Materials, University of Aveiro, Campus Universitário de Santiago, 3810-193 Aveiro, Portugal

[4] Center for Mechanical Technology and Automation—TEMA, Department of Mechanical Engineering, University of Aveiro; Campus Universitário de Santiago, 3810-193 Aveiro, Portugal

[*] Correspondence: r.j.ball@bath.ac.uk; Tel.: +44-1225-386944

Abstract: The solid-gas phase photo-catalytic activities of rutile TiO_2 and TiO_n (1<n<2) sub-oxide phases have been evaluated. Varying concentrations of Ti^{3+} defects were introduced into the rutile polymorph of titanium dioxide through carbo-thermal reduction at temperatures ranging from 350°C to 1300°C. The resulting sub-oxides formed were characterized by X-ray diffraction, X-ray photoelectron spectroscopy, scanning electron microscopy, impedance spectroscopy and UV-visible diffuse reflectance spectroscopy. The presence of Ti^{3+} in rutile exposed to high reduction temperatures was confirmed by X-ray diffraction. In addition, a Ti^{3+}-Ti^{4+} system was demonstrated to enhance the photo-catalytic properties of rutile for the degradation of the air pollutants NO_2 and CO_2 under UV irradiation of wavelengths (λ) 376-387nm and 381-392 nm. The optimum reduction temperature for photo-catalytic activity was within the range 350-400 ºC and attributed to improved charge-separation. The materials that were subject to carbo-thermal reduction at temperatures of 350°C and 400°C exhibited electrical conductivities over one hundred times higher compared to the non-reduced rutile. The results highlight that sub-oxide phases form an important alternative approach to doping with other elements to improve the photo-catalytic performance of TiO_2. Such materials are important for applications such as self-cleaning where particles can be incorporated into surface coatings.

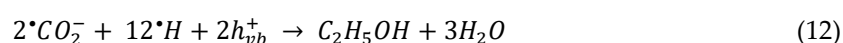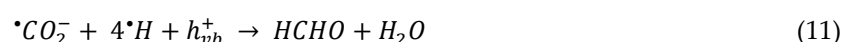**Keywords:** Photocatalysis; TiO_2; sub-oxide

1. Introduction

Following the discovery of water photo-splitting by Fujishima and Honda in 1972 [1] the properties of titanium dioxide have received much attention [2]. Research has focused on a diverse range of applications including wastewater treatment, reduction of atmospheric air pollutants and neutralisation of bacteria, fungus and other pathogens [3][4][5][6]. In addition to these, TiO_2 is also a key component in many self-cleaning technologies. Titanium dioxide is the natural oxide of Ti^{4+} (TiO_2) with the three main crystallographic structures being anatase, brookite and rutile [7][8][9][10]. Rutile is the most common polymorph of titania on Earth due to its thermodynamic stability and low molecular volume and much of the titanium dioxide in metamorphic and igneous rocks has a rutile crystal structure. While the optical band gap of anatase (3.2 eV) is higher than rutile (3.0 eV) [11].

The photo-catalytic reactions promoted by rutile remain of interest in both the gas and aqueous phase due to its abundance and widespread use. Aqueous based photo-catalysis studies, under UV light, include those focusing on the degradation of organic dyes and neutralisation of pathogens [2] [12].

Following the initial absorption of UV irradiation by the semiconducting rutile phase, an electron is promoted from its valence band to the conduction band over a femtosecond timescale [13]. This charge separation produces a reactive hole (h_{vb}^+) and associated electron (e_{cb}^-), this is shown in Equation 1. Both of these species may diffuse to the surface of the semiconductor and participate in a photo-catalytic reaction, provided they do not recombine forming an electron-hole pair. If the species are present on the surface, they can react with absorbed reduction and oxidation (red-ox) molecules leading to the formation of free radicals [1][14][15][16]. Equations 2-6 show typical reactions for H_2O and O_2 and those reactions which involve the formation of hydroxyl radicals and superoxide anions are the most important for pollution degradation, such as volatile organic compounds (VOCs) and NO_x via oxidation [6].

$$TiO_2 + h\upsilon \rightarrow h_{vb}^+ + e_{cb}^- \tag{1}$$

$$h_{vb}^+ + H_2O \rightarrow \ ^{\bullet}OH + H^+ \tag{2}$$

$$e_{cb}^- + H^+ \rightarrow \ ^{\bullet}H \tag{3}$$

$$e_{cb}^- + O_2 \rightarrow \ O_2^{\bullet-} \tag{4}$$

$$h_{vb}^+ + O_2^{\bullet-} \rightarrow \ ^1O_2 \tag{5}$$

$$H^+ + O_2^{\bullet-} \rightarrow \ HO_2^{\bullet} \tag{6}$$

Previous research on the surface of jet spray formed TiO_2 suggested reduction of CO_2 via reaction with an electron from the conduction band. The final reaction product formed following a number of reaction steps was proposed to be ethenolate [17]. In a different study the photocatalytic reduction of CO_2 in aqueous solution on surface-fluorinated anatase TiO_2 nanosheets with exposed {001} facets were investigated. Reduction of CO_2 was proposed to proceed via a mechanism involving generation of hydrogen radicals and carbon radicals where CO_2^- was formed extending the lifetime of photogenerated electron–hole pairs [18]. CO_2 photo reduction has also been proposed to consume electrons and hydrogen radicals as shown in Equations 7-12 [19], [20] [21], [22].

$$CO_2 + \ e_{cb}^- \rightarrow \ ^{\bullet}CO_2^- \tag{7}$$

$$^{\bullet}CO_2^- + \ 8^{\bullet}H + h_{vb}^+ \rightarrow \ CH_4 + 2H_2O \tag{8}$$

$$^{\bullet}CO_2^- + \ 6^{\bullet}H + h_{vb}^+ \rightarrow \ CH_3OH + H_2O \tag{9}$$

$$^{\bullet}CO_2^- + \ 2^{\bullet}H + h_{vb}^+ \rightarrow \ HCOOH \tag{10}$$

$$^{\bullet}CO_2^- + \ 4^{\bullet}H + h_{vb}^+ \rightarrow \ HCHO + H_2O \tag{11}$$

$$2^{\bullet}CO_2^- + \ 12^{\bullet}H + 2h_{vb}^+ \rightarrow \ C_2H_5OH + 3H_2O \tag{12}$$
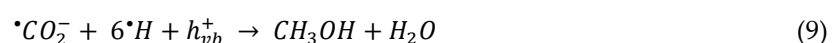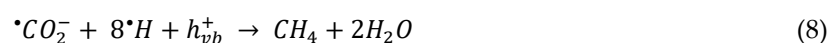
Halmann reported that one of the potential reasons why CO_2 reduction may occur in a less extensive percentage is the reoxidation of CO_2^- by hydroxyl radical [23][24]. Other studies suggested the mechanism involved the anchoring of CO_2 on the TiO_2 surface [25], [26].

In order to improve the photo-catalytic performance, research has explored a variety of approaches to shift the absorbance spectra towards the higher wavelengths of visible light. These approaches include (i) doping of the TiO_2, (ii) deforming its crystal lattice and (iii) tuning its bandgap [27][28][29][30]. Adding red-ox species, such as alcohols or ions such as Ag^+, also slows down the recombination of electrons and holes thereby reducing the carrier losses. An alternative strategy is to modify the electronic transfer properties of the material and involves improving the diffusion of charge to the material surface by increasing the bulk electrical conductivity.

In addition to the photocatalytic properties of TiO_2 another important phenomena observed is that of superhydrophillic behavior. When self-cleaning mechanisms are considered, on very flat surfaces, such as glass, the superhydrophillic properties of TiO_2 under UV irradiation can promote the formation of a thin water film rather than droplets, due to the reduced contact angle. This promotes the water film to run off the glass surface readily during which dirt particles are carried with it due to surface tension effects. However, this process is less likely to occur on rough or porous construction materials such as cement renders, lime renders, or the surface of concrete. On these rougher surfaced materials photocatalytic particles are added to the wet-mix. Following application of the cement, particles are left exposed on the surface following hardening or setting which impart self-cleaning properties due to the chemical degradation of dirt particles at the surface [31]. It is noteworthy that this mechanism is effective for organic contaminants containing bonds which can be attacked by the free radicals formed on the TiO_2 surface under light irradiation. The process efficiency is linked to the photocatalytic properties of the material.

In this paper we explore the approach of increasing the charge transfer towards the surface by reducing Ti^{4+} to Ti^{3+} to form sub-oxides and increase its electrical conductivity [32][33]. A variety of methods can be used to prepare titanium sub-oxides including hydrogenation [34][35], thermal treatment under an inert atmosphere [36], or by solvo-thermal methods employing $TiCl_3$ and TiF_4 [37]. This research investigates how vacancies in the rutile lattice of carbo-thermally reduced titania influence the phase structure, band gap, electrical conductivity and solid-gas photo-catalytic decomposition of nitrogen dioxide (NO_2) and carbon dioxide (CO_2) greenhouse gases. Photo-catalytic performance was evaluated under radiation of two different wavelength ranges, 376–387 and 381–392 nm, emitted from ultraviolet LED's. The effectiveness of these sub-oxide materials to decompose NO_2 is related to the free radicals formed on the surface. As it is these same radicals which react with other organic contaminates on the surface this can also reflect the self-cleaning potential.

2. Materials and Methods

Materials were formed from commercial TiO_2 rutile powder (0.3mm mean particle size, 99.5% pure, Pi-kem, UK) which was processed by the addition of 2.5%wt of an organic binder (polyethylene glycol-PEG 8000). By adding 1%v/w of distilled water to the powder, a slurry was formed and ball milled in a Capco machine for 24h at 120rpm [38][39]. Ball milling reduced the particle size and thoroughly mixed the organic binder with the ceramic powder preventing the formation of agglomerates. The slurry was subsequently dried and the resulting powder sieved through a 45μm mesh [40]. TiO_2 specimens were formed by dry cold pressing at a pressure of 250MPa (20kN over an area of 100mm^2). The resulting green body was then pressure-less sintered in a furnace at 1300°C in air for 90 minutes with an initial dwell at 400°C for 2 hours to decompose the binder. This firing regime was previously optimised to maximise the density (98.65±0.48% of theoretical) and control grain growth (5-10μm) [41]. To introduce Ti^{3+} defects into the structure of the TiO_2 a carbo-thermal reduction was employed, Equation 13 [42].

$$nTiO_2 + \frac{1}{2}C \rightarrow Ti_nO_{2n-1} + \frac{1}{2}CO_2 \tag{13}$$

Carbo-thermal reduction of the sintered titania was performed in a tube furnace (LTF, Lenton, UK), under a constant flow of argon to prevent re-oxidation. A micro-environment was created by embedding the specimens in carbon powder consisting of needle shaped particles of mean diameter 3.55μm and length 105μm. The reduction treatment started with a heating ramp of 150°C/h followed by a reduction stage of 24h. A range of reduction temperatures was employed to vary the degree of reduction; these temperatures included 350, 400, 450, 600 and 1300°C; a reduction temperature of 1300°C is typical for the manufacture of highly reduced Magnéli phases [36][43]. Once the reduction was complete, samples were cooled to room temperature with a ramp of 150°C/h. Further details describing the methodology for producing the sub oxide phases are available in PhD thesis [44].

The density of the samples was determined using the Archimedes method as described in the standard BS EN623:2.26 [45]. Theoretical densities (Dt) for TiO_2 and TiO_n were assumed to be 4.26g/cm^3 [46] and 4.30g/cm^3 respectively.

X-ray diffraction analysis (XRD) was used to determine the crystalline phase composition of the specimens. XRD was carried out using a BRUKER D8 ADVANCE X-ray diffractometer with CuK$_\alpha$ radiation (1.5406 Å), 2θ range between 20° and 140° with a step size of 0.016° 2θ and a virtual time-per-step of 200s. The microstructure of the specimens' surface was evaluated using a JEOL-JSM64802V scanning electron microscope (SEM) with an accelerator voltage of 15kV and a spot-size of 30nm. Specimens were coated with a 10nm layer of chromium to prevent surface charging. Rietveld refinement method was used for a fine study of oxygen occupancy.

X-ray photoelectron spectroscopy (XPS) was used to measure the surface elemental composition. The system was equipped with a hemispherical electro energy analyser (SPECS Phoibos 150), a delay-line detector and a monochromatic AlK$_\alpha$ (1486.74 eV) X-ray source. High resolution spectra were recorded at normal emission take-off angle and with a pass-energy of 20eV. The binding energies were corrected by referencing C-C to 284.8eV. The optical bandgap energy of the materials was determined using UV-Vis diffuse reflectance spectroscopy, along with the Kubelka-Munk function [34] (Eq. 14) to convert the reflectance, R, into the absorption coefficient, *F(R)*.

$$F(R) = (1 - R)^2 / 2R \tag{14}$$

Combining the Kubelka-Munk function with the Tauc's plot provides the absorption energy which corresponds to the bandgap, *E_g*, calculated from Equation 15,

$$(hv \times F(R))^2 = A \times (hv - E_g) \tag{15}$$

In addition to the bandgap, the diffuse reflectance spectrogram at 650nm was used to assign the intervalence charge transfer (IVCT) transition between Ti^{3+} and Ti^{4+}, where *h* is Planck's constant, *υ* is frequency of vibration and '*A*' is a proportionally constant. The bandgap was calculated from absorption spectra obtained at room temperature using a PerkinElmer 750 S UV/Vis Spectrometer with a 60mm integrating sphere in a wavelength range between 240nm and 800nm [33].

The effect of level of reduction and Ti^{3+} on the ac conductivity within the specimen bulk was determined by impedance spectroscopy. Electrical properties of stoichiometric titanium dioxide and sub-oxide species were characterized using a Solartron 1260 Impedance Analyser with a Solartron 1296 Dielectric Interface. Measurements were taken at frequencies from 1-10^5 Hz with a voltage perturbation of 0.1V$_{rms}$.

The photo-catalytic activity of the TiO_n specimens was evaluated by following the decomposition of CO_2 and NO_2 under UV illumination over a duration of 150 minutes in a reaction chamber coupled to an electron ionization mass spectrometer, as shown in Figure 1. 190ppm of NO_2, 6% of air balanced N_2 was introduced into the chamber followed by vacuum cycles up to 10^{-3} mbar to ensure the chamber

filled with the gas mixture and was not diluted by the gas previously in the chamber. Under these conditions three separate experiments were conducted, in the dark and under UV LED's emitting light of wavelength (λ) 376-387nm and 381-392nm. Experiments in the dark provided a comparison for absorption of gas onto the surface. Variations were shown to be within the background noise of the measurements. Further details can be found in the PhD thesis, Photocatalytic coatings in the built environment [47].

Data from the mass spectrometer was processed using a multiplicative approach using argon as an inert internal standard to avoid time-deviation errors [10]. The fractional change of inert argon during the experiment is defined as α, Eq. 16, where the superscript 'max' is the maximum value of its partial pressure for the data series; 'min' is the minimum value of its partial pressure for the data series and 'i' is the partial pressure value for a given time during the experiment. A similar approach to data is then used relating to the relative change in molecule X of interest (e.g. CO_2 or NO_2); defined as 'ε_x' in Eq. 17. This treatment normalises the data to a value between 0 and 1. The fractional change of 'X' considering the changes of Ar with time by the area of the sample in the Ar partial pressure scale is then defined by Eq. 18.

$$\alpha = \frac{(Ar^{max} - Ar^i)}{(Ar^{max} - Ar^{min})} \tag{16}$$

$$\varepsilon_X = \frac{(X^{max} - X^i)}{(X^{max} - X^{min})} \tag{17}$$

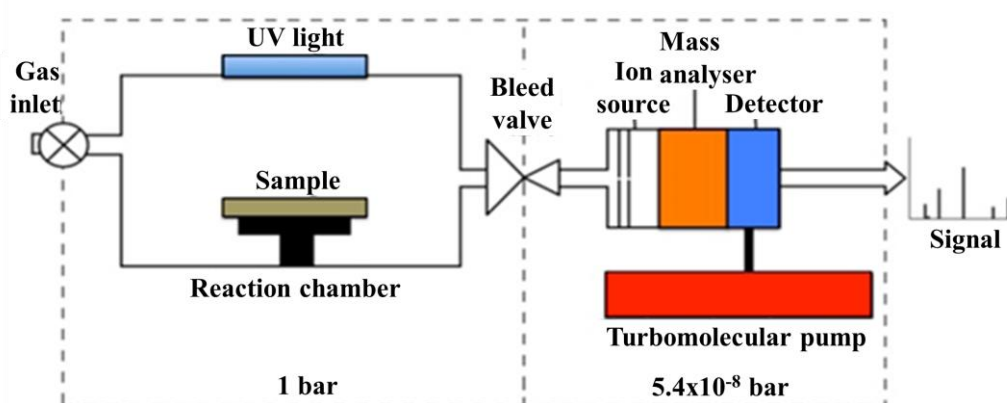$$_N^i X = (\varepsilon_x - \alpha)/Area \tag{18}$$

Figure 1. Schematic of the instrument for photo-catalytic activity

After 150 minutes, the fractional change value of the component 'X' for the reaction under UV was subtracted from the fractional change value of 'X' from the control experiment with no specimen in the chamber. This approach was then applied to determine the changes of CO_2 and NO_2 with time under dark and illumination conditions.

3. Results and discussion

3.1 X-ray characterisation and electron microscopy

Crystalline phases were identified from the X-ray patterns. The XRD diffractogram, shown in Figure 2 indicates that rutile was the main crystallographic phase, even for the specimen reduced at 1300°C where Magnéli phases (Ti_4O_7, Ti_6O_{11}) were present. The presence of secondary phases (i.e. sub-stoichiometric TiO_{2-x}) in specimens reduced within the temperature range 350-600 °C was not detected; if present, these phases, related to defects within the TiO_2 lattice, are therefore below the

detection limit of the XRD system (approximately 5%). Nevertheless, the presence of defects in reduced specimens, particularly Ti^{3+}, is confirmed by the changes in electrical conductivity measured by impedance spectroscopy, to be discussed in section 3.3.
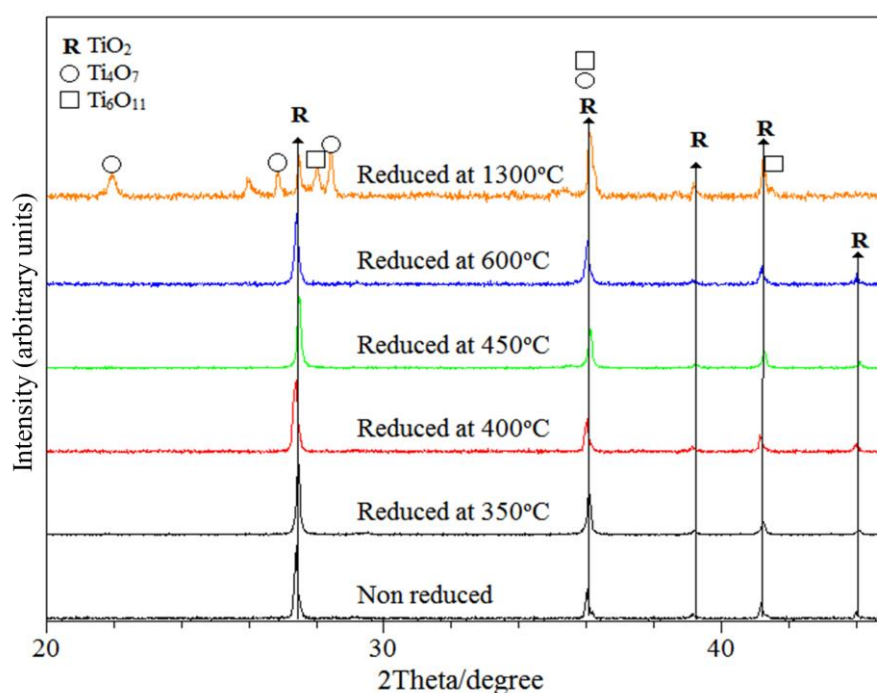

Figure 2. XRD diffraction patterns of non-reduced rutile and TiO_n carbo-thermally reduced from 350 °C to 1300 °C.

Changes in specimen microstructure as a result of the reduction temperature was examined by scanning electron microscopy, revealing no significant changes in structure from the non-reduced TiO_2 and specimens reduced at temperatures up to 600°C. Figures 3a and b show the surface morphologies of the non-reduced TiO_2 (theoretical density ~98.6%) and Magnéli phase based material reduced at 1300 °C (theoretical density ~96.7%) respectively. Due to the increased conductivity and diffusion processes during the reduction of TiO_2, there is significant grain growth when the material is reduced at this high temperature. The carbon-thermal reduction process leads to a gradual darkening on the materials as the reduction temperature increases; see insets Figures 3a and 3b.
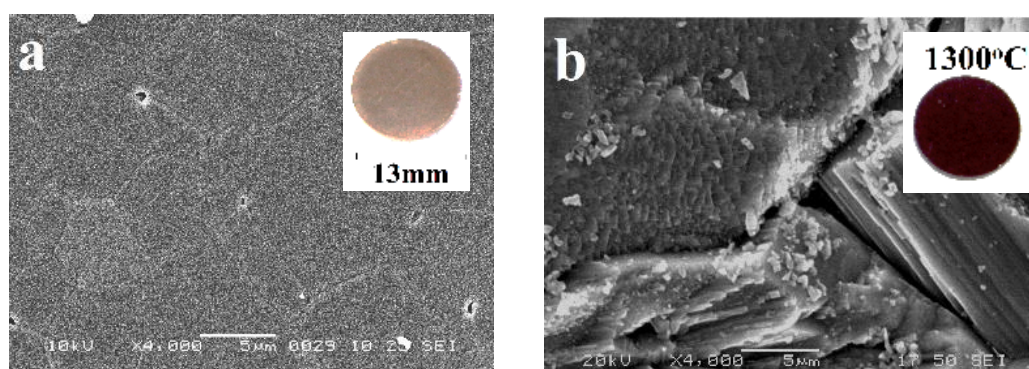

Figure 3. SEM images at same scale of (a) non-reduced TiO_2, (b) TiO_2 carbo-thermally reduced at 1300 °C. Inset shows colour change of material.

Figures 4a and 4b show the X-ray photoelectron spectra (XPS) obtained from the samples in the Ti 2p and O 1s regions. In the case of the non-reduced samples, Ti $2p_{3/2}$ presents a sharp component centered at a binding energy (BE) of 458.1 eV. This value shifted 0.5eV towards lower binding

energies for the samples prepared at higher temperatures 600⁰C and 1300⁰C of Figure 4a. Complementary, this shift was also detected in the O 1s core level as it is shown in Figure 4b, where the small component on the right of the spectra is ascribed to the oxygen atoms in the TiO_2 structure. These results are in good agreement with previous works in which the shift to lower BEs were ascribed to a reduction process [48].
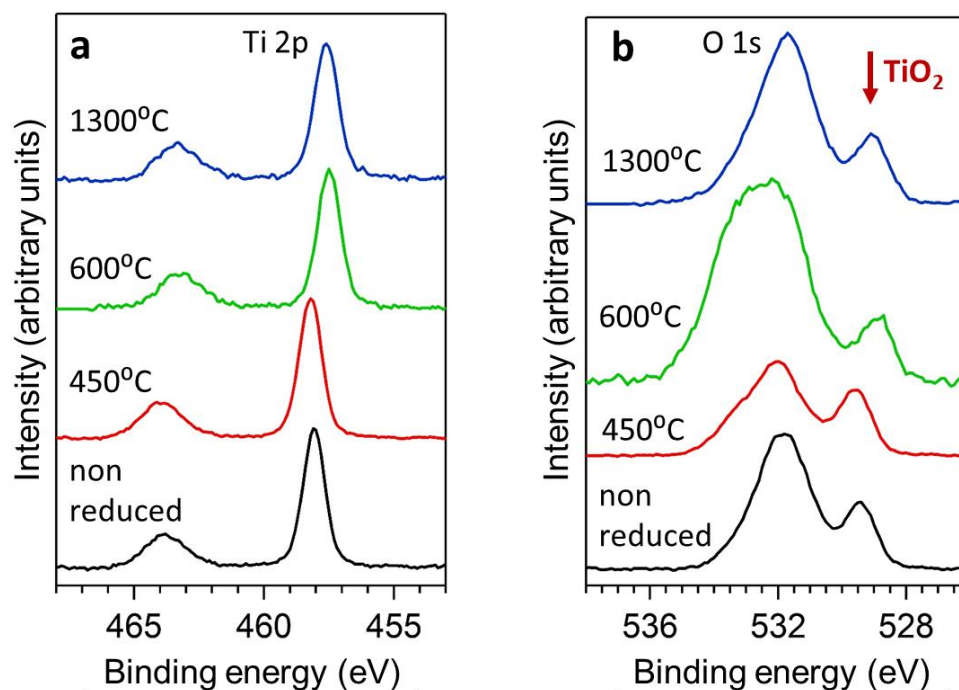

Figure 4. X-ray photoelectron spectra in the Ti 2p (a) and O 1s (b) regions of non-reduced rutile and TiO_n carbon-thermally reduced from 450°C to 1300°C.

3.2 UV-visible diffuse reflectance spectroscopy

Changes in band gap with reduction conditions, were identified by the application of the Kubelka-Munk model, however this was not applicable for the sample reduced at 1300°C containing significant conducting Magnéli phase as it was no longer a semiconductor; see impedance data in Section 3.3. Only small changes in the band gap were observed with the maximum corresponding to the specimen reduced at 400 ºC, see Table 1.

Table 1. Optical band gap of TiO_n specimens

Specimen - reduction temp	Band gap (eV)	Rietveld refinement for Oxygen vacancies
Rutile TiO_2	3.03	1
TiO_n-350 ºC	3.04	1
TiO_n-400 ºC	3.06	1
TiO_n-450 ºC	3.04	1
TiO_n-600 ºC	3.05	0.95
TiO_n-1300 ºC	Overlapped bands	-

The diffuse reflectance spectra in figure 5 revealed an absorption band at 650 nm for the samples reduced at 450°C which can be assigned to the intervalence charge transfer transition Ti^{3+} to Ti^{4+}.
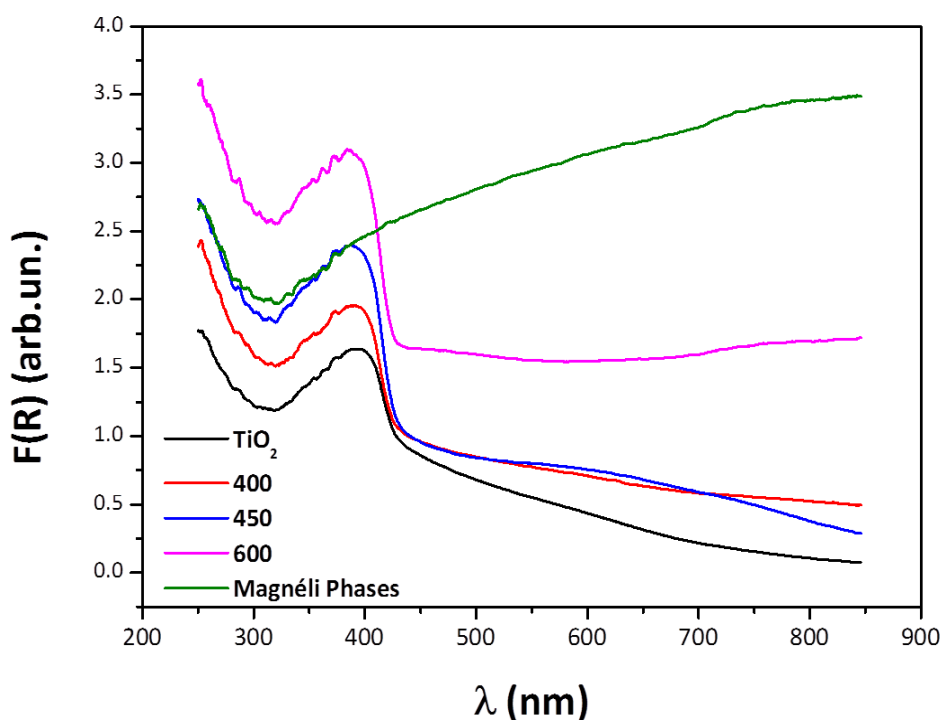
Figure 5. – Diffuse reflectance spectra for rutile and reduced samples

3.3 Electrical characterization

Impedance spectroscopy was performed to identify correlations between the ac conductivity and the photo-activity of the specimens. Figure 6a shows that the ac conductivity of the non-reduced rutile phase rises almost linearly with frequency and in this case the material is behaving predominately as a dielectric and the phase angle approaches -90° since current in a capacitor (dielectric) leads the voltage; see Figure 6b. For the carbo-thermally reduced materials there is an increase in the low frequency conductivity with increasing reduction temperature, see Figure 6a. Materials reduced at 350-400 °C exhibit the 'universal dielectric response' (UDR) whereby at low frequency the bulk ac conductivity is frequency independent, σ_{dc}, while at higher frequencies the ac conductivity increases following a power law behavior [49][50]. The higher electrical conductivity with increasing reduction temperature is a clear indication that by increasing the reduction temperature, a larger number of defects is introduced within the rutile lattice. It can therefore be concluded that, although the presence of Ti^{3+} could not be detected by XRD, a reduction temperature of 350°C is sufficient to form Ti^{3+} states.

In specimens reduced at 450°C to 1300°C the defects are the dominant phase and the conductivity response is frequency independent and the materials no longer exhibit the UDR, Figure 6a. This behaviour is much like that of a resistor with the phase angle approaching 0° and current and voltage are in phase, Figure 6b. Figure 6c shows the relative permittivity of selected materials as a function of frequency. The non-reduced rutile phase exhibits a relatively frequency independent permittivity, typical of a dielectric. The materials reduced at 350°C and 400°C show a significantly enhanced relative permittivity (in excess of 103) and strong frequency dependence. Materials reduced at 450-1300°C showed excessive noise in the permittivity data due to the high conductivity; e.g. see data for 600°C where the relative permittivity was 10^4-10^5; such as enhancement in permittivity, and frequency dependence has been shown to originate from conductivity in the material.

Changes in the conductivity are also shown in Figure 6d, illustrating the frequency dependence of the complex impedance, again indicating the transition from capacitive behaviour to restive

behaviour as the material is carbo-thermally reduced with a corresponding increase in electrical conductivity; this can be seen as a decrease in the real part of impedance (Z′) at low frequencies (right hand side intercept of the Z′-axis).
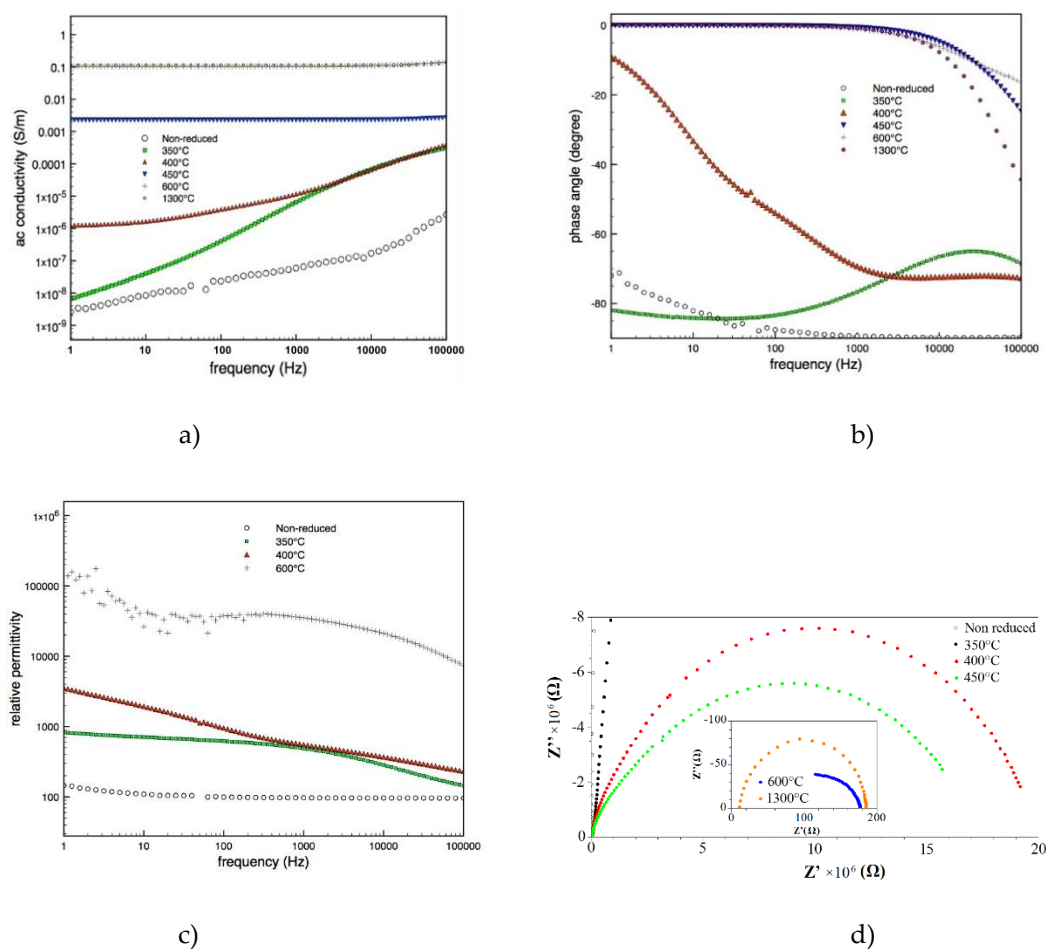

a)

b)

c)

d)

Figure 6. (a) AC conductivity (b) phase angle (c) permittivity, (d) complex plane plot of real impedance (Z′) vs imaginary impedance (Z′′) for TiO_n specimens.

3.4 Photo-catalytic performance

The degradation of CO_2 and NO_2 was monitored over 150 minutes through the fractional change relative to Ar for rutile and titanium sub-oxides. The sub-oxides were produced by reduction of rutile at temperatures ranging from 300°C to 1300°C. Two independent experiments were conducted using irradiation from LED's with wavelengths ranging from 376-387nm and 381-392nm. Figure 7 (a) and (b) present results showing the fractional change of CO_2 under wavelengths of 376-387nm and 381-392nm respectively. Figure 8 (a) and (b) present results showing the fractional change of NO_2 under wavelengths of 376-387nm and 381-392nm respectively. The results show an increase of photo-activity for both NO_2 and CO_2 when subjected to irradiation at wavelengths of 381-392nm for the titanium sub-oxide sample reduced at 400°C; see Figures 7b and 8b. The maximum degradation of NO_2 was observed for the titanium sub-oxide reduced at 350°C when irradiated with a wavelength of 376-387nm; see Figure 8a.

Based on these results it is thought that when the TiO_2 was not reduced the defects introduced within the rutile lattice are insufficient to induce a significant change in the conductivity of TiO_2 and improve charge-separation. The low frequency ac conductivity for the sample reduced at 350°C increased by

a factor of 10^1, compared to non-reduced rutile, see Figure 6(c), and up to 10^3 for the sample reduced at 400°C, leading to enhanced photo-activity.

This increase in the conductivity, due to the presence of Ti^{3+} in the bulk, can improve the efficiency of the electron-hole separation and stabilisation of the charge distribution. As a result, the photo-activity of the material increased. When the material was subjected to a greater degree of reduction, i.e. at reduction temperatures above 450°C, a much higher concentration of defects is produced which leads to localisation of defects, promoting recombination of charge carriers and therefore reducing the photo-activity. Tailoring the degree of reduction therefore offers a route to balance these effects to produce improved photo-catalytic materials.
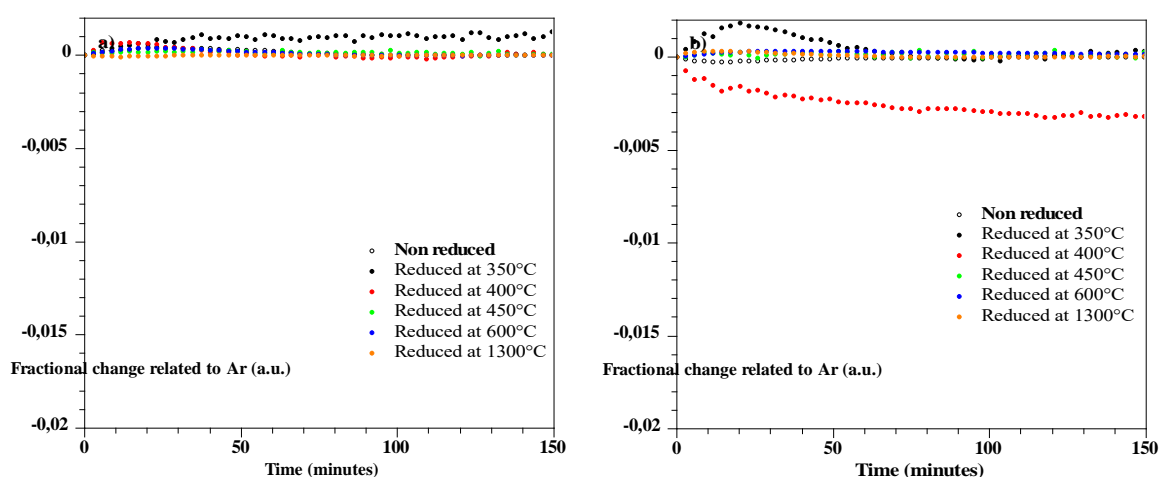

Figure 7. Fractional change of CO_2 over 150 minutes under UV of wavelengths (a) 376-387nm and (b) 381-392nm.
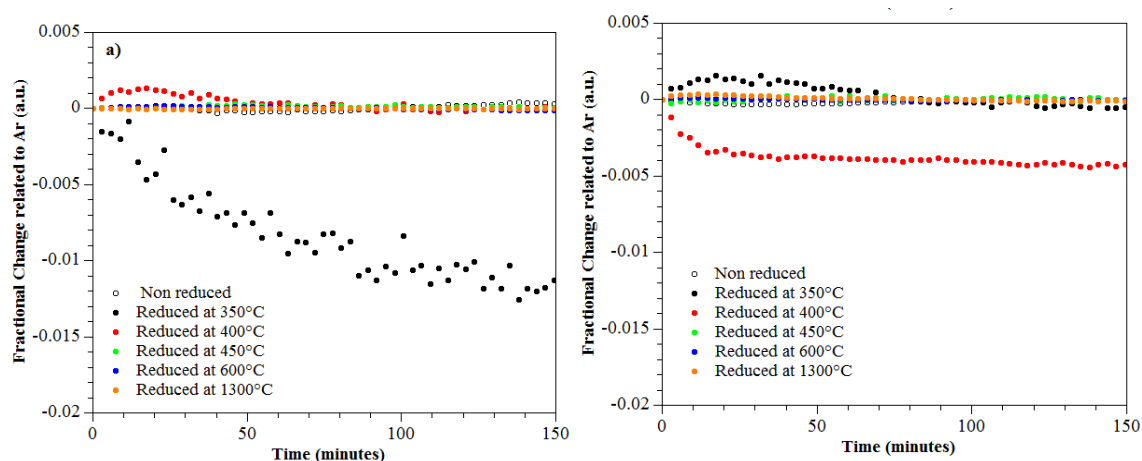

Figure 8. Fractional change of NO_2 over 150 minutes under UV wavelengths of (a) 376-387nm and (b) 381-392nm.

4. Conclusions

This paper has demonstrated that solid-gas phase solar photo-catalysis of rutile based materials can be enhanced by production of TiO_n (1<n<2) phases prepared by carbo-thermal reduction under an inert atmosphere. Materials were formed by carbo-thermal reduction of rutile at temperatures from 350°C to 1300°C and characterised in detail. The optimum temperature range to enhance photo-catalytic properties was 350°C to 400°C and demonstrates that the photo-catalytic performance of TiO_2 can be improved by the introduction of defects into the lattice by a reduction process.

The enhancement in solid-gas phase photo-activity for the degradation of CO_2 and NO_2 was attributed to the increase in the electrical conductivity; this leads to an improved separation of photo-generated charge carriers. Subjecting rutile to reduction temperatures 450°C and above lead to a significant increase in conductivity and created localized titanium sub-oxide species leading to the promotion of recombination of charge carriers and therefore does not lead to enhanced photo-activity. Impedance spectroscopy has proven to be the most suitable technique to measure titanium sub-oxide dislocations due to its sensitivity. This strategy constitutes an important alternative to doping TiO_2 with other elements to modify the band gap and thus photo-catalytic performance for applications such as air purification.

Author Contributions: Conceptualization, M. Nuño, R. J. Ball and C. R. Bowen.; Methodology, M. Nuño, R. J. Ball and C. R. Bowen.; XRD, D. M. Tobaldi.; XPS, M. J. H. Gallo and G. Otero-Irurueta.; Writing-Original Draft Preparation, M. Nuño, C. R. Bowen, D. M. Tobaldi, V. Adamaki, and R. J. Ball; Supervision, R. J. Ball and C. R. Bowen.; Project Administration, R. J. Ball and C. R. Bowen.; Funding Acquisition, R. J. Ball.

Conflicts of Interest: The authors declare no conflict of interest.

References:

[1]   A. Fujishima and K. Honda, "Electrochemical photolysis of water at a semiconductor electrode," *Nature*, vol. 238, pp. 37–38, 1972.

[2]   G. Meinhold, "Rutile and its applications in earth sciences," *Earth-Science Rev.*, vol. 102, no. 1–2, pp. 1–28, Sep. 2010.

[3]   H. Zhang and J. F. Banfield, "Thermodynamic analysis of phase stability of nanocrystalline titania," *J. Mater. Chem.*, vol. 8, no. 9, pp. 2073–2076, 1998.

[4]   A. Giampiccolo, M. P. Ansell, D. M. Tobaldi, and R. J. Ball, "Synthesis of Co–TiO_2 nanostructured photocatalytic coatings for MDF substrates," *Green Mater.*, vol. 4, no. 4, pp.

140–149, 2016.

[5]   M. Nuño, R. J. Ball, C. R. Bowen, R. Kurchania, and G. D. Sharma, "Photocatalytic activity of electrophoretically deposited (EPD) TiO_2 coatings," *J. Mater. Sci.*, vol. 50, no. 14, 2015.

[6]   A. Giampiccolo *et al.*, "Sol gel graphene/TiO_2 nanoparticles for the photocatalytic-assisted sensing and abatement of NO2," *Appl. Catal. B Environ.*, vol. 243, pp. 183–194, Apr. 2019.

[7]   D. M. Tobaldi *et al.*, "Quantitative XRD characterisation and gas-phase photocatalytic activity testing for visible-light (indoor applications) of KRONOClean 7000®," *RSC Adv.*, vol. 5, no. 124, 2015.

[8]   D. Reyes-Coronado, G. Rodríguez-Gattorno, M. E. Espinosa-Pesqueira, C. Cab, R. de Coss, and G. Oskam, "Phase-pure TiO_2 nanoparticles: anatase, brookite and rutile," *Nanotechnology*, vol. 19, no. 14, p. 145605, Apr. 2008.

[9]   A. Fujishima, X. Zhang, and D. Tryk, "TiO_2 photocatalysis and related surface phenomena," *Surf. Sci. Rep.*, vol. 63, no. 12, pp. 515–582, Dec. 2008.

[10]   M. Nuño, R. J. Ball, and C. R. Bowen, "Study of solid/gas phase photocatalytic reactions by electron ionization mass spectrometry," *J. Mass Spectrom.*, vol. 49, no. 8, pp. 716-726, 2014.

[11]   X. Liu *et al.*, "UV and visible light photoelectrocatalytic bactericidal performance of 100% {111} faceted rutile TiO_2 photoanode," *Catal. Today*, vol. 224, pp. 77–82, Apr. 2014.

[12]   A. Fujishima and X. Zhang, "Titanium dioxide photocatalysis: present situation and future approaches," *Comptes Rendus Chim.*, vol. 9, no. 5–6, pp. 750–760, May 2006.

[13]   A. Fujishima, T. N. Rao, and D. A. Tryk, "Titanium dioxide photocatalysis," *J. Photochem. Photobiol. C Photochem. Rev.*, vol. 1, no. 1, pp. 1–21, Jun. 2000.

[14]   O. Carp, C. L. Huisman, and A. Reller, "Photoinduced reactivity of titanium dioxide," *Prog. Solid State Chem.*, vol. 32, no. 1–2, pp. 33–177, 2004.

[15]   S. Wei, B. Peng, L. Chai, Y. Liu, and Z. Li, "Preparation of doping titania antibacterial powder by ultrasonic spray pyrolysis," *Trans. Nonferrous Met. Soc. China*, vol. 18, no. 5, pp. 1145–1150, Oct. 2008.

[16]   H. Nishikiori, Y. Fukasawa, Y. Yokosuka, and T. Fujii, "Nitrogen doping into titanium dioxide by the sol-gel method using nitric acid," *Res. Chem. Intermed.*, vol. 37, no. 8, pp. 869–881, 2011.

[17]   J. W. MacFarlane and T. B. Scott, "Reduction of carbon dioxide on jet spray formed titanium dioxide surfaces," *J. Hazard. Mater.*, vol. 211–212, pp. 247–254, Apr. 2012.

[18]   Z. He *et al.*, "Photocatalytic reduction of CO_2 in aqueous solution on surface-fluorinated anatase TiO_2 nanosheets with exposed {001} facets," *Energy and Fuels*, vol. 28, no. 6, pp. 3982–3993, Jun. 2014.

[19] Y. H. Inoue Hiroshi ,Matsuyama Takehiko, Liu Bi-Jin, Sakata Takao, Mori Hirotaro, "Photocatalytic Activities for Carbon Dioxide Reduction of TiO_2 Microcrystals Prepared in SiO_2 Matrices Using a Sol–Gel Method," *Chem. Lett.*, vol. 23, no. 3, p. 4, 1994.

[20] S. K. & K. H. Tooru Inoue, Akira Fujishima, "Photoelectrocatalytic reduction of carbon dioxide in aqueous suspensions of semiconductor powders," *Nature*, vol. 277, pp. 637–638, 1979.

[21] E. Bahadori A. Tripodi, A. Villa, C. Pirola, L. Prati, G. Ramis, and I. Rossetti, "High Pressure Photoreduction of CO_2: Effect of Catalyst Formulation, Hole Scavenger Addition and Operating Conditions," *Catalysts*, vol. 8, no. 10, p. 430, Sep. 2018.

[22] Y. Taniguchi, H. Yoneyama, and H. Tamura, "Photoelectrochemical Reduction of Carbon Dioxide at p-Type Gallium Phosphide Electrodes in the Presence of Crown Ether," *Bull. Chem. Soc. Jpn.*, vol. 55, no. 7, pp. 2034–2039, Jul. 1982.

[23] B. Aurian-Blajeni, M. Halmann, and J. Manassen, "Photoreduction of carbon dioxide and water into formaldehyde and methanol on semiconductor materials," *Sol. Energy*, vol. 25, no. 2, pp. 165–170, 1980.

[24] C. D. Jaeger and A. J. Bard, "Spin trapping and electron spin resonance detection of radical intermediates in the photodecomposition of water at titanium dioxide particulate systems," *J. Phys. Chem.*, vol. 83, no. 24, pp. 3146–3152, Nov. 1979.

[25] M. Anpo, H. Yamashita, Y. Ichihashi, and S. Ehara, "Photocatalytic reduction of CO_2 with $H2O$ on various titanium oxide catalysts," *J. Electroanal. Chem.*, vol. 396, no. 1–2, pp. 21–26, Oct. 1995.

[26] M. Anpo *et al.*, "Photocatalytic reduction of CO_2 with $H2O$ on Ti-MCM-41 and Ti-MCM-48 mesoporous zeolite catalysts," *Catal. Today*, vol. 44, no. 1–4, pp. 327–332, Sep. 1998.

[27] T. Ohno, T. Tsubota, K. Nishijima, and Z. Miyamoto, "Degradation of Methylene Blue on Carbonate Species-doped TiO_2 Photocatalysts under Visible Light," *Chem. Lett.*, vol. 33, no. 6, pp. 750–751, 2004.

[28] Y. Mizukoshi, N. Ohtsu, S. Semboshi, and N. Masahashi, "Visible light responses of sulfur-doped rutile titanium dioxide photocatalysts fabricated by anodic oxidation," *Appl. Catal. B Environ.*, vol. 91, no. 1–2, pp. 152–156, Sep. 2009.

[29] Y. Ren, J. Li, and J. Yu, "Enhanced electrochemical performance of TiO_2 by Ti^{3+} doping using a facile solvothermal method as anode materials for lithium-ion batteries," *Electrochim. Acta*, vol. 138, pp. 41–47, Aug. 2014.

[30] W. H. Saputera, G. Mul, and M. S. Hamdy, "Ti^{3+}-containing titania: Synthesis tactics and photocatalytic performance," *Catal. Today*, vol. 246, pp. 60–66, May 2015.

[31] M. Nuño, G. L. Pesce, C. R. Bowen, P. Xenophontos, and R. J. Ball, "Environmental performance of nano-structured $Ca(OH)_2/TiO_2$ photocatalytic coatings for buildings," *Build.*

Environ., vol. 92, pp. 734–742, 2015.

[32]   M. Xing, W. Fang, M. Nasir, Y. Ma, J. Zhang, and M. Anpo, "Self-doped Ti^{3+}-enhanced TiO_2 nanoparticles with a high-performance photocatalysis," *J. Catal.*, 2013.

[33]   S. Riyapan, Y. Boonyongmaneerat, O. Mekasuwandumrong, P. Praserthdam, and J. Panpranot, "Effect of surface Ti^{3+} on the sol–gel derived TiO_2 in the selective acetylene hydrogenation on Pd/TiO_2 catalysts," *Catal. Today*, vol. 245, pp. 134–138, May 2015.

[34]   V. Adamaki, F. Clemens, P. Ragulis, S. R. Pennock, J. Taylor, and C. R. Bowen, "Manufacturing and characterization of Magnéli phase conductive fibres," *J. Mater. Chem. A*, vol. 2, no. 22, pp. 8328–8333, 2014.

[35]   Q. Zhu Y. Peng, L. Lin, Cong-Min Fan, Gui-Qi Gao, Rui-Xia Wang and An-Wu Xu., "Stable blue TiO_{2-x} nanoparticles for efficient visible light photocatalysts," *J. Mater. Chem. A*, vol. 2, no. 12, p. 4429, 2014.

[36]   S. R. Sangawar, J. P. Agarwal, and D. B. Sarwade, "A comprehensive study on some binders for piezo-electric ceramics," *Indian J. Eng. Mater. Sci.*, vol. 8, no. 1, pp. 26–35, 2001.

[37]   F. Bradley, "The Relation of Ceramics Processing to Materials Properties for Electronic Applications," *IEEE Trans. Parts, Hybrids, Packag.*, vol. 8, no. 4, pp. 15–23, Dec. 1972.

[38]   M. N. Rahaman, *Ceramic Processing*. CRC Press, 2017.

[39]   S. J. Kalita, S. Qiu, and S. Verma, "A quantitative study of the calcination and sintering of nanocrystalline titanium dioxide and its flexural strength properties," *Mater. Chem. Phys.*, vol. 109, no. 2–3, pp. 392–398, 2008.

[40]   F. C. Walsh and R. G. A. Wills, "The continuing development of Magnéli phase titanium sub-oxides and Ebonex® electrodes," *Electrochim. Acta*, vol. 55, no. 22, pp. 6342–6351, Sep. 2010.

[41]   P. C. S. Hayfield, *Development of a New Material*. Cambridge: Royal Society of Chemistry, 2007.

[42]   W. E. Wang and Y. S. Kim, "Thermodynamic evaluation of the titanium-oxygen system from O/Ti = 0 to 3/2," *J. Nucl. Mater.*, vol. 270, no. 1, pp. 242–247, 1999.

[43]   K. P. Surendran, P. V. Bijumon, P. Mohanan, and M. T. Sebastian, "(1-x)$MgAl_2O_4$-xTiO_2 dielectrics for microwave and millimeter wave applications," *Appl. Phys. A*, vol. 81, no. 4, pp. 823–826, Sep. 2005.

[44]   V. Adamaki, "Manufacturing and characterisation of Ti-suboxides for sensing and energy applications", PhD Thesis, University of Bath, 2015.

[45]   R. López and R. Gómez, "Band-gap energy estimation from diffuse reflectance measurements on sol–gel and commercial TiO_2: a comparative study," *J. Sol-Gel Sci. Technol.*, vol. 61, no. 1, pp. 1–7, Jan. 2012.

[46] D. S. McClure, "Mineralogical applications of crystal field theory by R. G. Burns," *J. Appl. Crystallogr.*, vol. 3, no. 6, pp. 550–550, Dec. 1970.

[47] M. Nuño, "Photocatalytic coatings in the built environment", PhD Thesis, University of Bath, 2015.

[48] Q. Kang, J. Cao, Y. Zhang, L. Liu, H. Xu, and J. Ye, "Reduced TiO2 nanotube arrays for photoelectrochemical water splitting," *J. Mater. Chem. A*, vol. 1, no. 18, p. 5766-5774, 2013.

[49] D. P. Almond and B. Vainas, "The dielectric properties of random R - C networks as an explanation of the `universal' power law dielectric response of solids," *J. Phys. Condens. Matter*, vol. 11, no. 46, pp. 9081–9093, Nov. 1999.

[50] D. P. Almond and C. R. Bowen, "Anomalous Power Law Dispersions in ac Conductivity and Permittivity Shown to be Characteristics of Microstructural Electrical Networks," *Phys. Rev. Lett.*, vol. 92, no. 15, p. 157601, Apr. 2004.